Performance evaluation of a vibration desensitized scanning white light interferometer

2014 Surf. Topogr.: Metrol. Prop. 2 014011

(http://iopscience.iop.org/2051-672X/2/1/014011)

IOP Publishing Surface Topography: Metrology and Properties
Surf. Topogr.: Metrol. Prop. **2** (2014) 014011 (8pp) doi:10.1088/2051-672X/2/1/014011

Performance evaluation of a vibration desensitized scanning white light interferometer

J Troutman, C J Evans, V Ganguly and T L Schmitz

Center for Precision Metrology, Department of Mechanical Engineering and Engineering Science, UNC Charlotte, 9201 University City Boulevard, Charlotte, NC 28223, USA

E-mail: jtrout13@uncc.edu

Received 9 August 2013, revised 9 December 2013
Accepted for publication 11 December 2013
Published 30 December 2013

Abstract

Surface metrology instruments normally require thermal, seismic and acoustic isolation. Shop-floor metrology solutions offer reduced cost and process time. If they operate on the same principles as laboratory devices, an inherent sensitivity to vibration remains. This paper describes a methodology for evaluating 'environmental tolerance' and applying it to characterize a recently introduced 'environmentally tolerant' scanning white light interferometer (SWLI). Previously published measurements of replicated nickel reference standards on the new instrument and on a stylus profilometer showed good correlation. Surface topography repeatabilities (per ISO 25178-604:2013) were insignificantly different when evaluated on the SWLI instrument in a metrology laboratory and in a manufacturing area. Measurements of reference standards under forced vibration of the entire instrument show maximum ripple error and data dropout in regions of structural resonance. Measurements were performed with large forced horizontal and vertical sample oscillation beneath the objective, exhibiting maximum ripple error near odd integer multiples of half the instrument detector frequency. Error due to data dropout was also investigated.

Keywords: interferometry, vibration, frequency response, surface roughness

1. Introduction

Shop-floor metrology solutions offer numerous advantages, including cost and process time reduction, over their laboratory counterparts. Most instruments designed for surface metrology are sensitive to environmental effects and, therefore, are typically installed in metrology laboratories offering the required thermal, seismic and acoustic isolation. While no instrument can be completely immune to environmental effects, an 'environmentally tolerant' scanning white light interferometer (SWLI) has recently been introduced. If this instrument and its laboratory counterparts operate on the same basic principles, a similar response to environmental disturbances can be expected for both. While desensitized instruments may exhibit lower magnitude responses to vibration, the degree of 'environmental tolerance' is seldom quantified. Although theoretical models for the response to seismic excitation of some generic instrument types are well-defined in the literature, experimental evaluations are lacking. This paper describes a methodology for evaluating the sensitivity of a 'tolerant' instrument to seismic and environmental vibration using a commercial SWLI. High quality surfaces were measured as a test case.

Scanning white light interferometry (also known as coherence scanning interferometry, or CSI (ISO 25178-604:2013)) has evolved into a widely used technique for rapid areal assessment of a variety of surfaces [1]. SWLI typically operate by translating the reference leg of the interferometer to modulate interference fringe phase between the collection of multiple interferograms (intensity frames), which can be used to compute surface topography. Instruments with long coherence illumination are classified as phase-shifting interferometers (PSI), while short coherence length variants are referred to as SWLI or CSI instruments. De Groot [2] presents a mathematical treatment of the effect of random-phase vibration on PSI instruments for

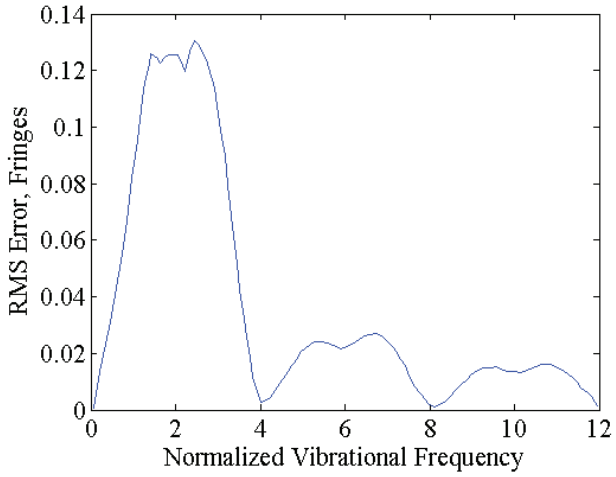

Figure 1. Rms error as a function of frequency for $\lambda/4$ phase shifting interval, horizontal axis normalized to one-fourth detector frequency (Hz).

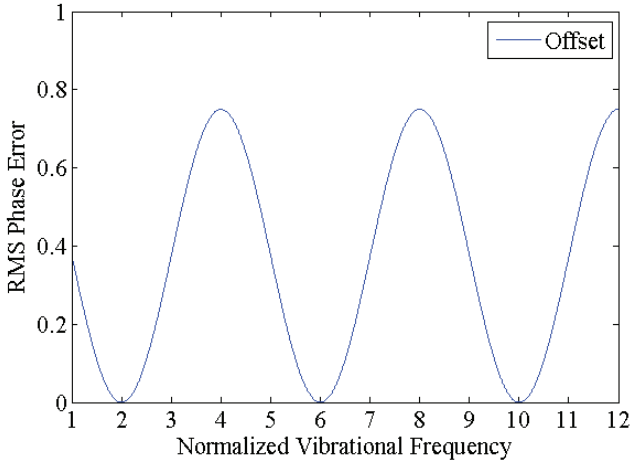

Figure 2. Rms error due to offset. Vertical axes normalized to vibration amplitude, horizontal axes to one-fourth detector frequency (Hz).

various computational algorithms. Random vibration along the measurement axis of PSI instruments produces two error types: (i) constant fringe phase shift; and (ii) ripple at twice the fringe frequency. In [3], de Groot develops and experimentally verifies a numerical simulation for PSI with varying algorithms. Figure 1 shows predicted rms error for the three-bucket algorithm applied on an instrument with a phase-shifting interval of one-quarter fringe. The horizontal axis is normalized to one-fourth the detector frequency.

For the three-bucket algorithm, the simplest approach to PSI, rms phase errors due to offset and ripple are shown as a function of frequency in figures 2 and 3 for the case of continuous phase shifting, a technique which is becoming more practical with the availability of high-speed digital cameras. Park [4] and Kimbrough [5] demonstrate improved vibration desensitization using continuous phase shifting.

Although the approach described in this paper can be applied to any instrument, all data was collected using a Zygo ZeGage ZG100 optical profiler. Previous work,

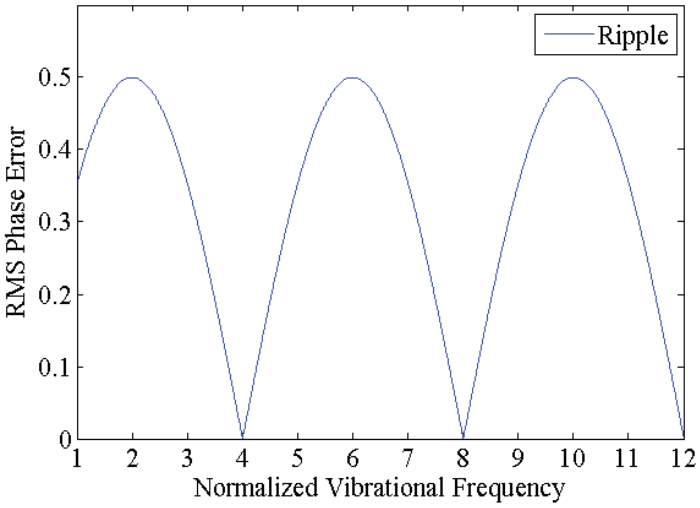

Figure 3. Rms error due to ripple. Vertical axes normalized to vibration amplitude, horizontal axes to one-fourth detector frequency (Hz).

Table 1. Surface repeatability at varied magnification for laboratory and shop floor environments.

Magnification	Sq (lab) (μm)	Repeatability (lab) (μm)	Repeatability (shop) (μm)
5×	0.567	0.035	0.028
20×	0.530	0.031	0.042
50×	0.647	0.038	0.023

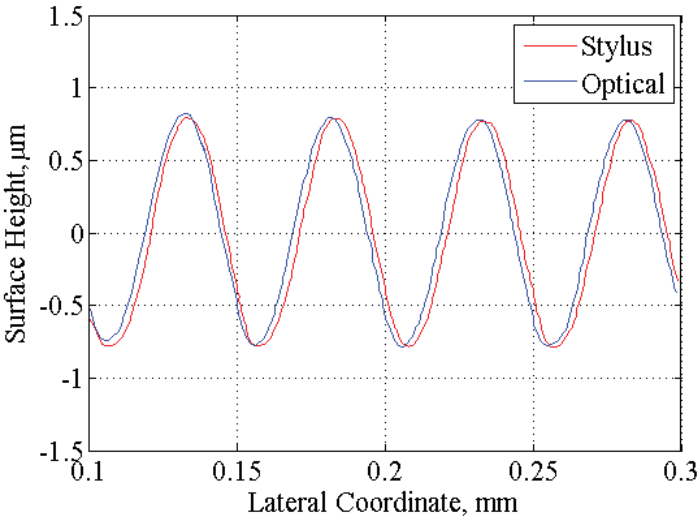

Figure 4. (right) Comparison of stylus and optical profiles for a Rubert 528× sinusoidal specimen, measured at 20×. A small phase shift has been added, redrawn from [6].

summarized in table 1 and figure 4, showed good correlation between results obtained with the desensitized instrument and separate profilometer measurements of replicated reference standards [6].

Continuing the initial work from [7], measurements made in the machine shop with the instrument within 1 m of milling machines running high stock removal process with spindle speeds both above and below the camera frame rate

Table 2. Sa error for turned Ti sample.

Drive (Hz)	Sa (μm)	Error (%)
0	1.512	
50	1.516	0.20
100	1.505	0.46
150	1.405	7.10
180	1.194	21.0
225	1.245	17.0

of 100 Hz showed negligible degradation in metrological performance. Tests performed using an electric motor with a small unbalanced mass provided varying frequency and excitation amplitude as a function of motor speed. Table 2 shows the variation in Sa as a function of frequency. At 150 Hz, the amplitude of the vibration was 500 nm. The instrument exhibited data dropout, where certain pixels return a null value, at excitation frequencies of 180 and 225 Hz.

2. Structural response of instrument

The bulk of the available literature considers vibration along the instrument's optical axis, while real environments provide excitation along three orthogonal axes. Results of the initial work suggested that an evaluation of instrument performance at frequencies up to 300 Hz and amplitudes measured at the sample table under 500 nm would be appropriate, corresponding to the 'workshop' level of the vibration criterion (VC) specifications [8]. The evaluation begins with assessment of the instrument's structural dynamics. The instrument was placed on a rolling hydraulic cart to facilitate portability and simulate an industrial installation. Using the setup shown in figures 6(a)–(d), a modal shaker on the cart base was used for excitation, and frequency response functions were measured at the upper surface of the cart, the SWLI's sample table, and the SWLI objective mount.

The modal shaker was attached to the base using high-stiffness epoxy. Responses were collected using integrated circuit piezoelectric (ICP) high-sensitivity ($10\,\mathrm{V\,g^{-1}}$) accelerometers. A triaxial mounting block attached with wax was used to collect response at the cart and table, while a specially designed mounting block that threads into the objective mount, which, combined with the sensors, is of similar mass as the 50× objective, was used to collect response at the objective. Frequency response was determined using a swept-sine technique and was verified using pseudo-random broadband noise input. A right-handed coordinate system, as shown, is defined from the perspective of the observer in figure 6(a): $+Z$ points upward, $+X$ points to the right and $+Y$ points away from the viewer. For brevity, figure 5 presents only the relative table-objective motion as a function of frequency. Similar behaviour is evident along the X and Y axes; response peaks centred near 120 Hz occur for all input orientations, though are broader for Y axis response. X and Y response content centred near 210 and 280 Hz occur for all inputs, though at significantly higher amplitude for Z inputs, while responses near 320 and 340 Hz are significantly higher for Y inputs. The Z response can be described as uniform between 240 and 280 Hz for X input, and between 200 and 300 Hz for Y and Z inputs, with a defined peak at 250 Hz for Y inputs.

3. Instrument response to forced vibration

3.1. Error classification

As noted previously, vibration along the optical axis (Z) is expected to produce a phase offset and ripple. Relative motion between the objective and the sample in X and Y will, at minimum, result in similar errors, depending on the local slope. Other errors such as loss of contrast and, therefore, increased noise, will occur when X and Y motions are significant compared to the pixel size. Such errors have not been treated analytically in the literature and will not be considered further in this study.

A third error, data dropout, is seen as a vibration response. Only briefly described in the literature, data dropout refers to the instrument returning null (NaN) values for certain pixels. This occurs due to poor signal-to-noise ratio during phase modulation, in practice appearing in regions of high local slope. In an ideal environment, data dropout is minimized by selecting proper operating parameters (objective, scan distance). However, during forced vibration testing, dropout often occurs at certain frequencies for specimens where no dropout was evident at static condition.

While offset and ripple, as described by de Groot, are both real mathematical errors, the offset error is normally invisible to the operator, as a constant phase offset will result in the same indicated surface form and texture, only centred about a different mean plane. Most instruments remove this 'piston' error, as well as tip/tilt error, because they are generally considered setup errors. Therefore, this paper is confined to ripple and dropout errors, those immediately evident to the user. To demonstrate these errors, figure 7 shows the topography of a sinusoidal reference specimen (Rubert 543×), measured with a 50× objective and no forced vibration. Figure 8 shows ripple at twice the interference fringe frequency, as well as data dropout in regions of high local slope, for a vibration frequency of 125 Hz. Figure 9 illustrates the interference fringe orientation for these measurements. During this investigation, measurements were performed in a manufacturing environment equipped with high speed diamond turning, polishing and jig boring equipment, also subjected to office-level footfall from adjacent hallways and overhead. The measurement results presented here were performed with all machinery idle and during periods of minimized footfall. The instrument returns surface data as a 1024×1024 matrix of height values. When measuring with a 50× objective that provides a 166.6 μm square field of view, the Rubert 543× single frequency sinusoidal sample with 2.5 μm wavelength is sampled at 15 pixels per wave, corresponding to 0.13 times the Nyquist limit. For this spatial frequency, a typical instrument of this type will have a modulation transfer function of approximately 0.9 [9], indicating that the sine wave on this sample is adequately resolved.

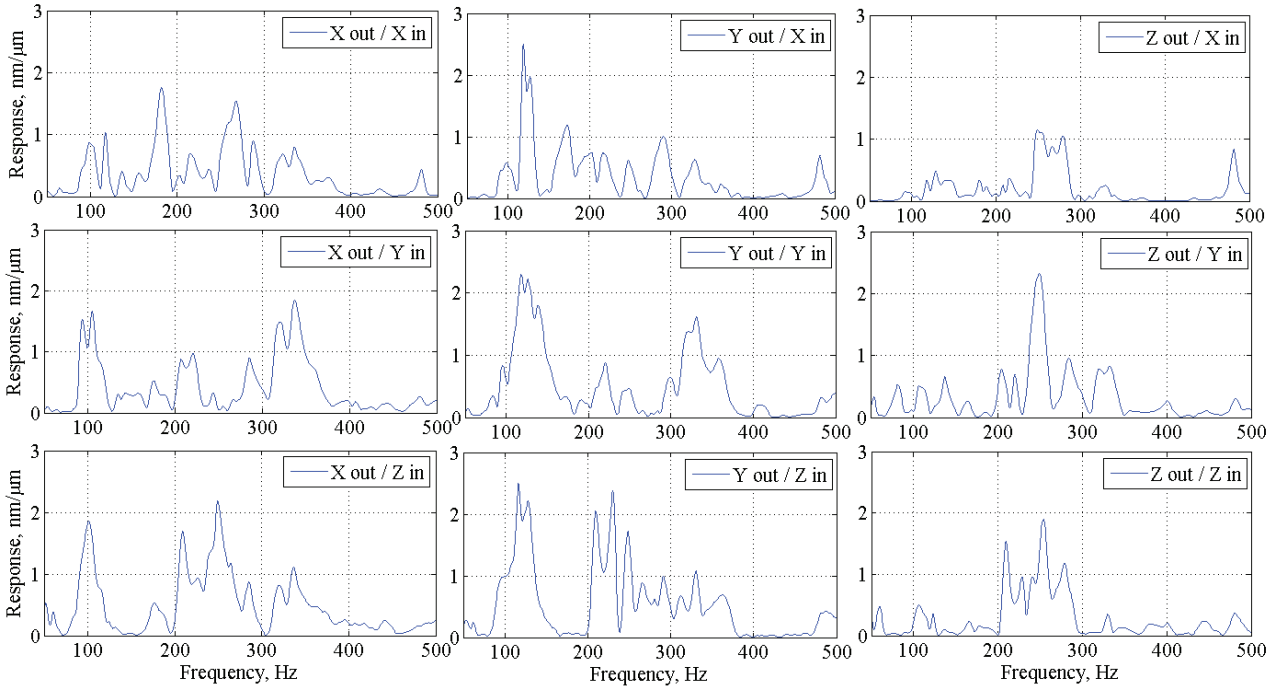

Figure 5. Relative table–objective motion. The vertical axis is normalized to the vibration amplitude/1000 (a value of 1 in the figure could indicate a motion response of 3 nm for a 3 μm vibration, e.g.).

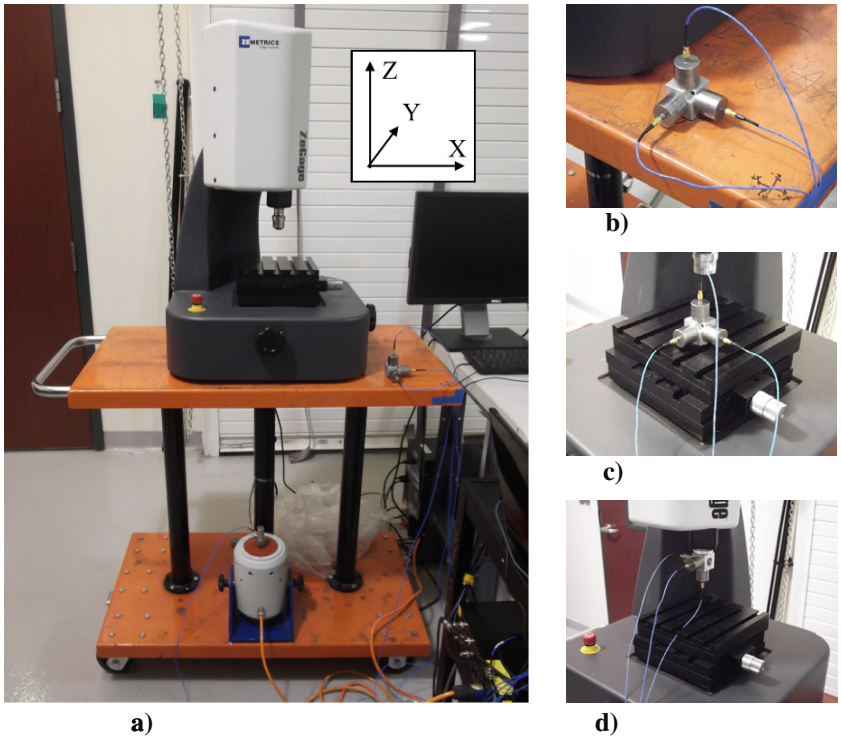

Figure 6. (a) SWLI on hydraulic cart, (b) cart sensors, (c) table sensors and (d) optics sensors.

3.2. Error quantification

Best practice operation of a micro-interferometer calls for 'nulling', or minimizing the number of fringes, to minimize retrace errors. As a side effect, nulling reduces the spatial frequency (but not the amplitude) of ripple errors. Here, multiple fringes are desired for easy visualization of the ripple error. Samples were oriented on the instrument with surface lay (for directional surfaces) and interference fringes nominally orthogonal to simplify analysis of ripple errors. Errors are quantified using MATLAB.

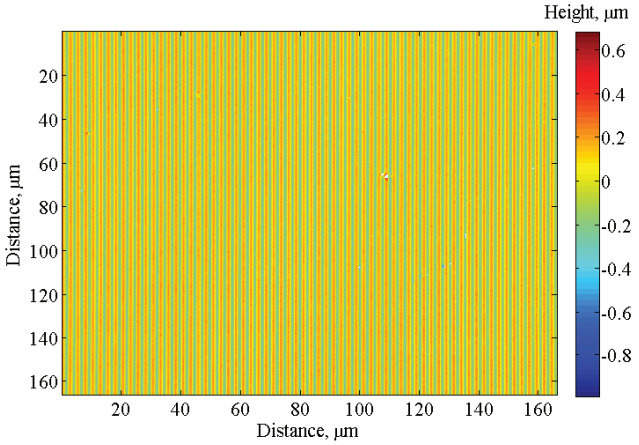

Figure 7. Static topography of specimen.

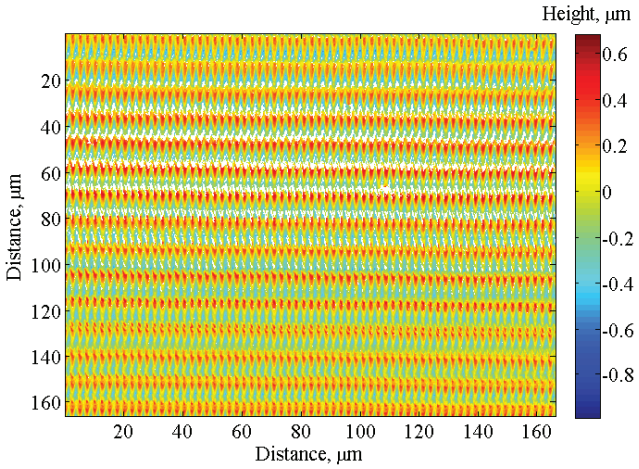

Figure 8. 125 Hz topography of specimen.

For the case of surface lay oriented vertically and fringes horizontally, measurement produces an $n \times n$ matrix $\boldsymbol{A}$, which is composed of n similar rows; the fast Fourier transform (FFT) of the mth column is denoted as

$$\mathcal{F}_m^{\boldsymbol{A}} = \mathrm{FFT}\left[\boldsymbol{A}_{1,m} \cdots \boldsymbol{A}_{n,m}\right]. \tag{1}$$

The rms of this column (which represents a single profile along the surface) can be found in the frequency domain from Parseval's theorem

$$\mathrm{rms}_m^{\boldsymbol{A}} = \sqrt{\frac{1}{\boldsymbol{n}^2} \sum \left|\mathcal{F}_m^{\boldsymbol{A}}\right|^2}. \tag{2}$$

Averaging this rms over p profiles is evenly distributed throughout $\boldsymbol{A}$:

$$\mathrm{rms}^{\boldsymbol{A}} = \frac{1}{\boldsymbol{p}} \sum_{q=1}^{\boldsymbol{p}} \mathrm{rms}_{q \cdot \boldsymbol{n}/\boldsymbol{p}}^{\boldsymbol{A}}. \tag{3}$$

For matrices $\boldsymbol{S}$ and $\boldsymbol{D}$, representing measurements at static and dynamic conditions, respectively, the rms error due to ripple is then

$$\boldsymbol{E}_{\mathbf{R}} = \left|\mathrm{rms}^{\boldsymbol{D}} - \mathrm{rms}^{\boldsymbol{S}}\right|. \tag{4}$$

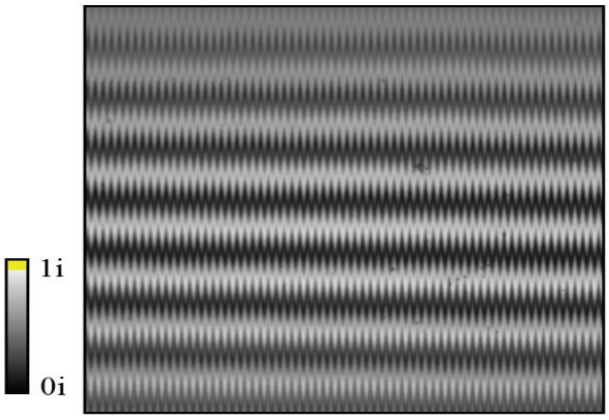

Figure 9. Interference fringe orientation.

Table 3. Specimens used for vibration response investigation.

Manufacturer	Specimen name	Type	Pitch (μm)	Measured Sa (μm)
Rubert	543×	Sinusoidal	2.5	0.060
Thorlabs	Mirror	Random	–	0.006

To quantify data dropout, define

$$\boldsymbol{N}_{i,j} = \begin{cases} 0 & \text{if} \quad \boldsymbol{S}_{i,j} \notin \mathbb{R}, \\ 1 & \text{if} \quad \boldsymbol{S}_{i,j} \in \mathbb{R} \quad \text{and} \quad \boldsymbol{D}_{i,j} \notin \mathbb{R}, \\ 0 & \text{otherwise.} \end{cases} \tag{5}$$

The data dropout percentage can then be specified as

$$\boldsymbol{E}_{\boldsymbol{D}} = \frac{100\%}{\boldsymbol{n}^2} \sum_{i,j=1}^{\boldsymbol{n}} \boldsymbol{N}_{i,j}. \tag{6}$$

3.3. Vibration response

To further examine the effects of forced vibration, a small electric shaker was placed on the instrument's base casting and output was measured with a high-sensitivity ICP seismic accelerometer ($10\,\mathrm{V\,g^{-1}}$). The specimen to be measured was clamped securely to the instrument's t-slotted table via a flat plate with Teflon sample clamps.

From 50 to 300 Hz, measurements were performed at 5 Hz increments with constant 50 nm amplitude as measured at the base casting, corresponding to a 300 nm vibration at the sample table at 210 Hz. At each frequency, the instrument was carefully focused and then the surface was measured with a 50× Mirau objective using a 30 μm scan length. Settings, such as scan speed and processing algorithm, are fixed and unchangeable for this instrument. Variations were found to occur depending on the vibration phase at the time of acquisition, so, to negate this effect, each measurement is an average of six data acquisitions. Three measurements were performed at each frequency. Table 3 describes the specimens.

As shown in figure 10, ripple error is maximum in areas of high relative sample–objective motion, as expected. To investigate the ripple dependence upon amplitude, the 543× and a nickel-plated mirror were measured at 210 Hz

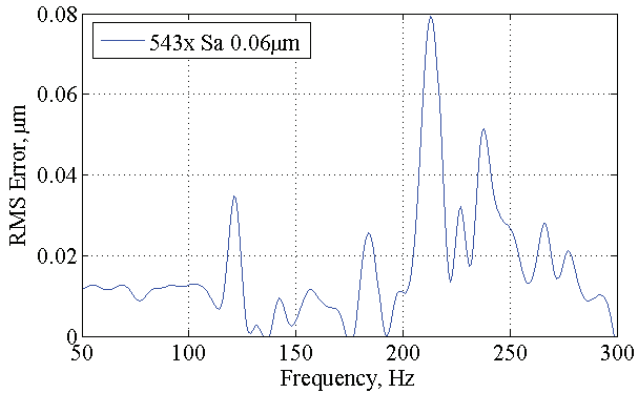

Figure 10. Vibration frequency dependence.

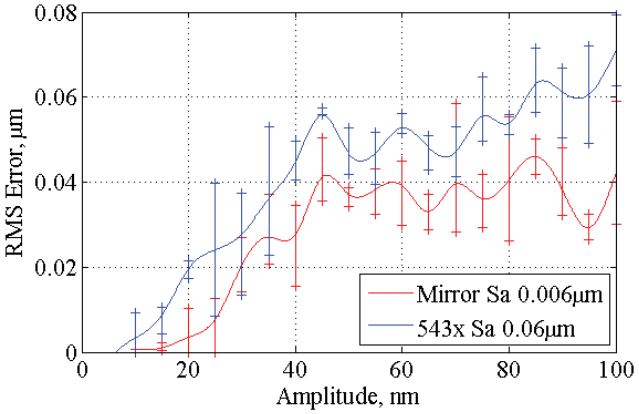

Figure 11. Vibration amplitude dependence.

(the region of highest ripple error) with vibration amplitudes between 10 and 100 nm as measured at the base casting. Figure 11 shows that the two samples are similar in their nonlinear behaviour with increasing amplitude. Error bars, showing the extrema of the three measurements, identify error repeatability on the order of ±50 nm. An increase in rms error with increasing specimen roughness is also evident.

4. Instrument response to forced sample–objective motion

4.1. Design of sample shakers

The response of the instrument to forced vibration indicated maximum error in areas of sample–objective motion. However, due to the structural dynamics of the instrument, the electric shaker was inappropriate for generating constant-amplitude relative motion at all frequencies. To overcome this test limitation, two flexure-based mechanisms were constructed which oscillate samples beneath the objective in both horizontal and vertical directions.

As shown in figures 12 and 13, these flexure mechanisms each use eight leaf-type flexures in parallel. Approximately 200 mm square in size, these sample shakers are actuated using a water-cooled, low-voltage piezoelectric actuator and are capable of generating sinusoidal motion in the 50–350 Hz range. Vibration amplitudes above 100 nm are feasible and

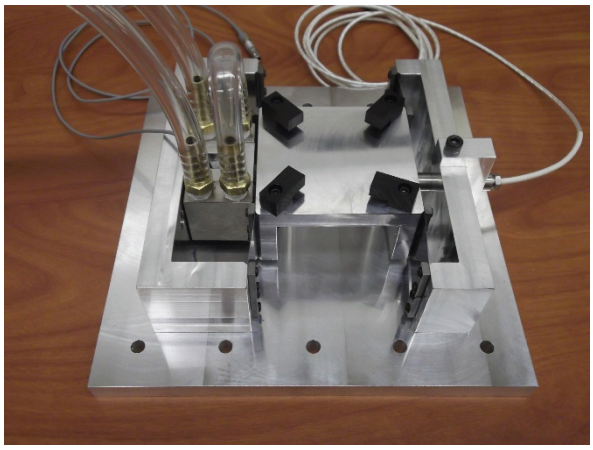

Figure 12. Horizontal sample shaker.

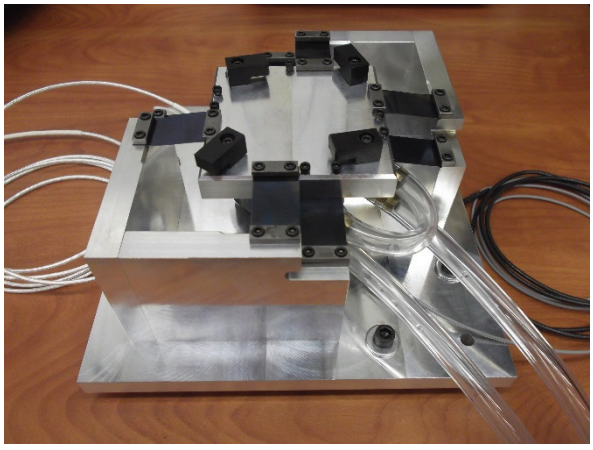

Figure 13. Vertical sample shaker.

controllable to within ±10 nm. Special care was taken to minimize torsional and off-axis motions, which are on the order of 1%. Displacement is sensed using capacitive probes and the shakers mount to the instrument table via t-nuts and cap screws. For all actuation orientations, these shakers result in a motion response at the instrument objective of 5–8% of shaker amplitude in regions of structural resonance.

4.2. Instrument response to vertical sample oscillation

To evaluate the SWLI response to vertical sample oscillation, the vertical sample shaker shown in figure 13 was used to oscillate the 543× and mirror specimens between 50 and 300 Hz with 5 Hz steps and constant output amplitude of 300 nm (a similar output condition to the forced vibration evaluation in regions of high resonance). As described previously, each measurement was an average of six data collections and each measurement was repeated three times. The measurements were performed using a 50× Mirau objective.

Figure 14 illustrates ripple error as a function of frequency for both specimens. Figure 15 illustrates data dropout. For both figures, the horizontal axis is normalized to one-fourth the detector frequency, which is 100 Hz for

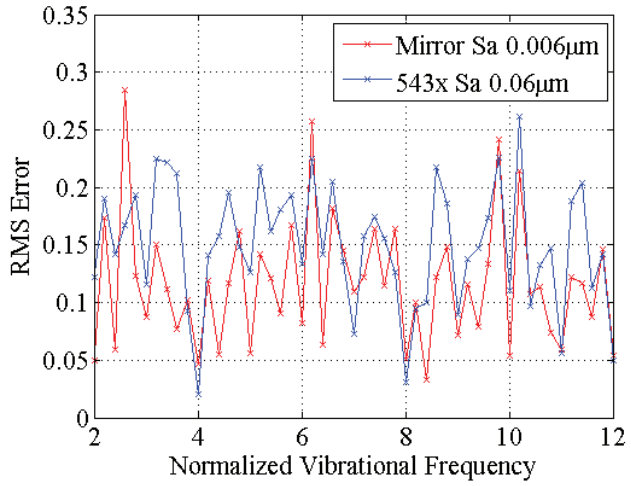

Figure 14. Ripple error for vertical oscillation, vertical axis normalized to vibration amplitude.

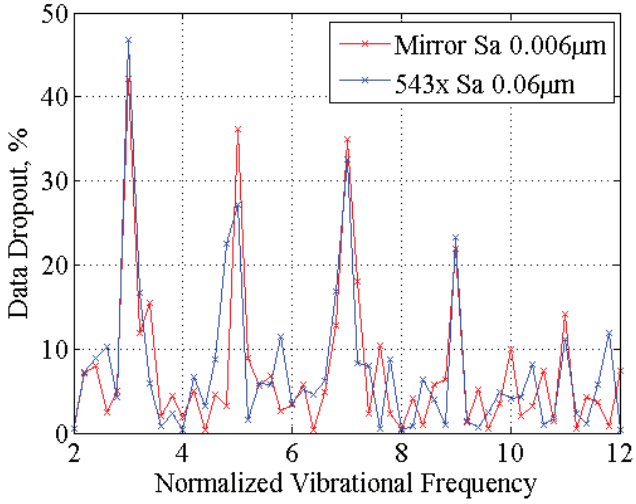

Figure 15. Data dropout for vertical oscillation.

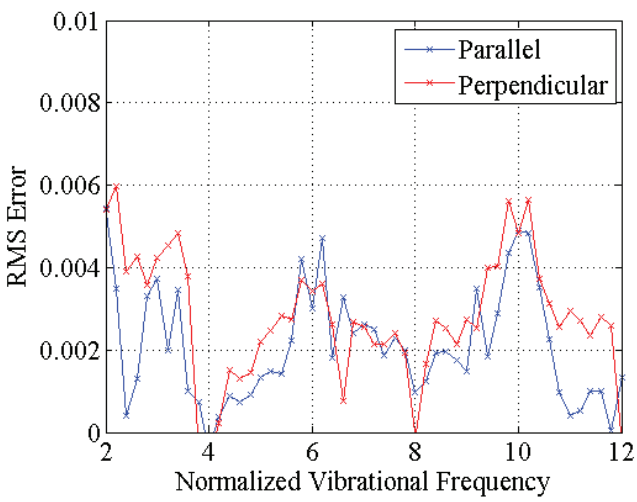

Figure 16. Ripple error for horizontal oscillation, vertical axis normalized to vibration amplitude.

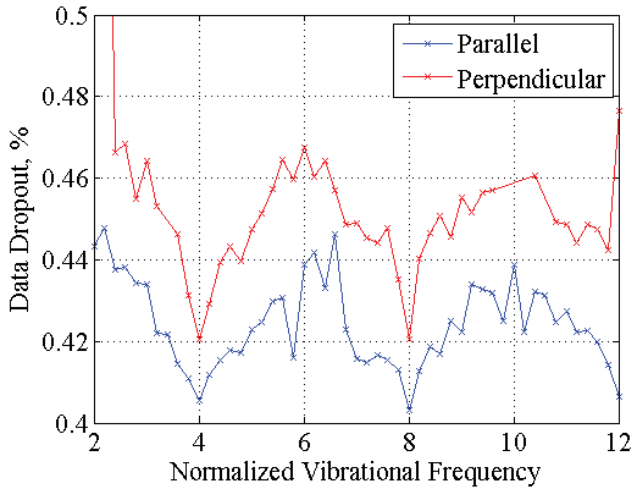

Figure 17. Data dropout for horizontal oscillation.

this instrument. The trend predicted by de Groot in figure 1 is satisfied, yet with lower amplitude than predicted. Data dropout decreases with increasing frequency and peaks at odd integer multiples of the detector frequency appear.

4.3. Instrument response to horizontal sample oscillation

The horizontal sample shaker shown in figure 12 was used to oscillate the mirror specimen at a 300 nm amplitude over the 50–300 Hz range. Referring to figure 9, the sample was evaluated for horizontal motion both parallel and perpendicular to the interference fringes (left-to-right and top-to-bottom, respectively). Figure 16 shows rms error dependence on frequency for horizontal oscillation. Figure 17 shows data dropout percentage; again, for both figures, the horizontal axis is normalized to one-fourth the detector frequency. Unlike the case of vertical oscillation, over this range, ripple and data dropout are undetectable by eye.

As shown, rms errors due to ripple follow the same trend as vertical oscillation, but magnitudes are on the order of 1%. This ripple error can be attributed to the parasitic motion of the horizontal sample shaker; though the motion is nominally horizontal, small vertical oscillations also occur. For horizontal oscillation, data dropout follows the same trend as rms errors, with minima at multiples of the detector frequency and maxima at odd integer multiples of half the detector frequency. The rms errors for oscillation along both directions are behave in a similar manner, while data dropout is slightly higher for the case of motion perpendicular to the interference fringes.

5. Concluding remarks

The methods described in this paper can be applied to any instrument used for surface metrology. Although the instrument's response to forced sample oscillation can provide useful information to the metrologist, an operating environment can be specified simply from the target instrument uncertainty for a given application, the structural

dynamics of the instrument and its response to excitation frequency, which can be determined relatively quickly at low cost.

The environmentally tolerant SWLI evaluated in this paper exhibits maximum ripple error and data dropout in frequency regions producing maximum motion between the sample and objective. Below a certain threshold, rms error is approximately linear with vibration amplitude; above this threshold, approximately 50 nm as measured at the instrument base (corresponding to 300 nm sample–objective motion), dependence is nonlinear, but, in general, increases with vibration amplitude. As predicted by de Groot, forced vertical sample oscillation produces local rms error maxima at odd multiples of half the detector frequency. Forced horizontal sample oscillation results in a similar rms error trend, with magnitudes of approximately 1%, most likely due to the parasitic off-axis motion of the sample shaker and local slope of the sample.

The instrument manufacturer provided little guidance aside from suggesting a VC-C [8] or better operating environment, which seems conservative considering the results obtained here and elsewhere. VC-C is typically recommended for lithography and inspection equipment down to 1 μm feature size, while typical workshops can exceed this by factors of four or more. Also, VC criteria are only defined to an upper limit of 80 Hz, unsuitable for characterizing modern manufacturing shops, especially those using high-speed milling and similar processes.

Rms ripple errors below 2 nm and data dropout levels below 0.5% are undetectable to the operator's bare eye and are likely to have negligible effect on the parametric description of most surfaces. The data given here suggest that this level of metrological performance will be achieved if vibration as measured at the sample table does not exceed 50 nm amplitude for any frequency component.

A more complete specification for any instrument will require further evaluation. Though the test conditions in this investigation were chosen to simulate a manufacturing environment, the instrument response to vibration amplitudes on order of one-tenth to one-fifth fringe should be investigated for further comparison with [3]. The effect of magnification on instrument sensitivity should be explored by expanding this evaluation to include several objectives. Response to horizontal sample oscillation should be evaluated as a function of local slope by testing the response of multiple specimens. Environmental tolerance should be tested near operating machinery to verify response to environmental vibration at multiples of the detector frequency. Specifying an installation environment will require testing the instrument response to forced broadband noise. Passive and active noise isolation systems could also be explored for improvement of instrument response.

References

[1] de Groot P 2009 *Optical Measurement of Surface Topography* ed R Leach (Berlin: Springer) chapter 9, pp 187–208

[2] de Groot P 1995 Vibration in phase-shifting interferometry *J. Opt. Soc. Am.* A **12** 354–65

[3] de Groot P and Deck L 1996 Numerical simulations of vibration in phase-shifting interferometry *Appl. Opt.* **35** 2172–8

[4] Park J and Kim S 2010 Vibration-desensitized interferometer by continuous phase shifting with high speed fringe capturing *Opt. Lett.* **35** 19–21

[5] Kimbrough B, Brock N and Millerd J 2011 Dynamic surface roughness profiler *Proc. SPIE* **8126** 81260H

[6] Badami V, Liesener J, Evans C and de Groot P 2011 Evaluation of the measurement performance of a coherence scanning microscope using roughness specimens *Proc. ASPE Annual Meeting (Denver)* pp 23–6

[7] Evans C J, Troutman J, Ganguly V and Schmitz T 2013 Performance evaluation of a vibration desensitized scanning white light interferomter *Proc. 14th Int. Conf. on Metrology and Props of Engineering Surfaces (Taipei)* pp 232–8

[8] Gordon C G 1999 Generic vibration criteria for vibration-sensitive equipment *Proc. SPIE* **1619** 71–85

[9] Colonna de Lega X and de Groot P 2012 Lateral resolution and instrument transfer function as criteria for selecting surface metrology instruments *Imaging and Applied Optics Technical Digest* OTu1D.4 (Washington, DC: Optical Society of America)